Journal of Catalysis **209,** 6–15 (2002)
doi:10.1006/jcat.2002.3627

Mn-Promoted Ni/Al_2O_3 Catalysts for Stable Carbon Dioxide Reforming of Methane

Seung-Ho Seok,* Sun Hee Choi,* Eun Duck Park,* Sung Hwan Han,† and Jae Sung Lee*,[1]

*Department of Chemical Engineering, Pohang University of Science and Technology (POSTECH), San 31 Hyoja-Dong, Pohang 790-784, Republic of Korea; and †Environment and Process Technology Division, Korea Institute of Science and Technology (KIST), 39-1 Hawolgok-dong, Sungbuk-ku, Seoul 136-791, Republic of Korea

Received June 21, 2001; revised January 29, 2002; accepted March 18, 2002

Based on previous observation that the addition of manganese onto Ni/Al_2O_3 catalysts reduced the coke formation in the carbon dioxide reforming of methane, effects of the preparation method for Mn-promoted Ni/Al_2O_3 catalysts on the catalytic activity and stability were investigated. A coprecipitated catalyst, $Ni–MnO_x/MnAl_2O_4$, showed higher coke resistance and more stable activity than an impregnated $Ni/MnO/\gamma\text{-}Al_2O_3$ catalyst and the well-known $Ni_{0.03}Mg_{0.97}O$ catalyst at 923 K with a feed gas ratio CH_4/CO_2 of 1 without a diluent gas. In coprecipitated $Ni–MnO_x/MnAl_2O_4$ catalysts, $MnAl_2O_4$, $\gamma\text{-}Al_2O_3$, and Ni(0) were observed as major crystalline phases with XRD and potassium was detected on the surface with EPMA. Comparison of H_2 chemisorption and XRD suggested that the surface of large metallic nickel particles was partly blocked by manganese oxides, and the structure was confirmed by XAFS. For impregnated $Ni/MnO/\gamma\text{-}Al_2O_3$ catalysts, addition of potassium stabilized its catalytic activity further, to the level achieved by coprecipitated $Ni–MnO_x/MnAl_2O_4$ catalysts. These results indicate that very stable Ni/Al_2O_3 catalysts for the carbon dioxide reforming of methane can be prepared by addition of both potassium and manganese as promoters.

Key Words: **CO_2 reforming; methane; nickel catalysts; manganese; potassium; coke deposition.**

1. INTRODUCTION

There has been increased interest in the catalytic reforming of methane with carbon dioxide ("dry reforming") into synthesis gas ($CO_2 + CH_4 \rightarrow 2CO + 2H_2$) since it has the following advantages for the efficient utilization of those abundant materials.

1. Methane and carbon dioxide, well-known "greenhouse gases" (1), are converted into a valuable feed stock.
2. The product mixture of this reaction has a low H_2/CO ratio (1 : 1) that is desirable for direct use as a feedstock for the Fisher–Tropsch reaction to produce liquid fuels (2).
3. This reaction is considered for chemical energy transmission systems, in which a power source drives the endothermic reforming reaction, and the product gases are transported to consumers at remote areas, where the reverse exothermic methanation reaction can be performed (3).

Most group VIII metals, especially noble-metal- and Ni-based catalysts, have been studied for CO_2 reforming of methane (4). One major obstacle to the successful industrial application is the coke formation via the Boudouard reaction ($2CO \rightarrow C + CO_2$) and/or methane decomposition ($CH_4 \rightarrow C + 2H_2$), which leads to catalyst deactivation, plugging of the reactor, and breakdown of the catalyst. The catalysts based on noble metals have been reported to be more active and less sensitive to coking than Ni-based catalysts (5, 6). However, considering the high cost and limited availability of noble metals, it is more practical to develop Ni-based catalysts which are resistant to carbon deposition and exhibit high activity for the reaction.

Previous work on improving the coke resistance of Ni-based catalysts can be categorized as follows.

1. Carbon deposition can be suppressed when TiO_2 (7), La_2O_3 (8), or ZrO_2 (9) is used as a catalyst support.
2. It has been suggested that carbon deposition is suppressed when nickel is supported on a metal oxide with strong Lewis basicity (10).
3. The catalyst structure appeared to affect the carbon deposition. The formation of $NiAl_2O_4$ during the pretreatment procedure caused a marked decrease in coke deposition (11). Solid solution of NiO–MgO has been reported to enhance catalyst lifetime by decreasing carbon formation (12–17). This is related to the small nickel crystallites which are stable toward sintering and carbon formation (18, 19).
4. Some metal additives can preferentially eliminate the large ensembles of metal atoms necessary for carbon deposition (20, 21). This strategy has already been applied to the commercial SPARG process, in which Ni-based catalysts were partially poisoned with sulfur compounds to suppress carbon deposition while sacrificing its activity (22).

Recently we reported an interesting additive effect on the performance of a commercial nickel catalyst (ICI46-1)

[1] To whom correspondence should be addressed. Fax: 82-54-279-5528. E-mail: jlee@postech.ac.kr.

0021-9517/02 $35.00

(23). Various modifiers, such as Co, Cu, Zr, Mn, Mo, Ti, Ag, and Sn, were tested. The major role of these additives was to suppress the deposition of unreactive carbon ("coke"). The best effect in securing stability without sacrificing much activity was obtained when manganese was used as a modifying additive. Detailed studies on $Ni/MnO/\gamma\text{-}Al_2O_3$ catalyst revealed that the surface of nickel is partly covered ("decorated") by patches of MnO_x and that manganese addition also promotes the adsorption of CO_2 by forming a reactive carbonate species (24). Further study also indicated that the activity and the stability of Mn-containing Ni/Al_2O_3 catalysts were strongly dependent on the preparation method (25). Thus, in this paper, effects of the catalyst preparation method are investigated on CO_2 reforming of methane over this stable Mn-promoted Ni/Al_2O_3 catalyst.

2. EXPERIMENTAL

2.1. Catalyst Preparation

Ni/Al_2O_3 (17 wt%), 17 wt% Ni/ZrO_2, 17 wt% Ni/CeO_2, 17 wt% Ni/La_2O_3, 17 wt% Ni/MnO, and Ni–Mn–Al oxides (molar ratio, $Ni:Mn:Al = 1:1:6$; $Ni–MnO_x/MnAl_2O_4$) were prepared by a coprecipitation method. Metal nitrates were dissolved in distilled water and K_2CO_3 was added dropwise into this solution. When precipitation was completed, the slurry solution was aged at 333 K for 1 h and filtered and washed with hot distilled water several times. The filtered cake was dried at 393 K for 12 h and calcined at 1123 K for 10 h in air. All catalysts were crushed and the powder with sizes between 100 and 200 mesh was utilized for the reaction.

$Ni/\gamma\text{-}Al_2O_3$ (5 wt%), 5 wt% Ni/10 wt% $MnO/\gamma\text{-}Al_2O_3$, and promoted 5 wt% Ni/10 wt% $MnO/\gamma\text{-}Al_2O_3$ catalysts were prepared by a wet impregnation method from $\gamma\text{-}Al_2O_3$ (Strem $S_{BET} = 150\ m^2/g$) and metal nitrates. After impregnation, catalysts were dried overnight at 393 K and subsequently calcined at 973 K for 6 h.

Mn/ICI (3 wt%) (23) and $Ni_{0.03}Mg_{0.97}O$ (13) catalysts were prepared following the recipe reported previously.

2.2. CO_2 Reforming of Methane

Catalytic reaction runs were carried out using a conventional flow-type quartz reactor at atmospheric pressure. The sieved catalyst powder (100–200 mg) was evenly distributed over the quartz disk forming a bed 1–2 mm thick. A thermocouple connected to a PID temperature controller was placed on the top of catalyst bed. The reactant gas stream consisted of carbon dioxide and methane with a molar ratio of 1 : 1 flowing at a rate of 81.7 μmol/s. Prior to the reaction, the catalyst was usually reduced *in situ* at 1073 K, unless otherwise specified, for 1 h in dihydrogen flow and the activity was measured at 923 K. The reaction conditions were chosen such that external and internal mass transfer limitations were avoided (26). The gas compositions of reactants and products were analyzed by a gas chromatograph (Hewlett–Packard 5890) equipped with a packed-column (Porapack Q) and a thermal conductivity detector.

2.3. Characterization of Catalysts

N_2 adsorption/desorption isotherms at 77 K for prepared catalysts were obtained on a constant-volume adsorption apparatus (Micrometrics, Accusorb 2100E). The amounts of hydrogen chemisorption were determined on the same apparatus at room temperature.

Temperature-programmed desorption (TPD) of CO_2 was performed in flowing He (37 μmol/s) with a heating rate of 10 K/min after adsorption of CO_2 at room temperature. Temperature-programmed oxidation (TPO) was conducted for used catalysts in flowing 1% O_2/He with a heating rate of 10 K/min from room temperature to 1173 K.

The amount of carbon formed on catalysts during the reaction was determined by using a LECO CHNS-932 analyzer. Electron probe microanalysis (EPMA) was employed to determine the distributions of Ni, Mn, Al, and K with wavelength-dispersive spectroscopy (WDS) and quantitative analysis with energy-dispersive spectroscopy (EDS) on Jeol JXA-8600. For these analyses, samples were mounted on graphite stubs and gold was sputtered onto them to ensure adequate conductivity.

X-ray powder diffraction patterns were obtained at room temperature using a M18XHF(MAC Science Co.) with Ni-filtered Cu $K\alpha$ radiation with a wavelength of 1.54056 Å. The X-ray tube was operated at 40 kV and 200 mA. Samples were finely ground and packed into a glass holder having a $18 \times 18 \times 2$ mm opening. No adhesive or binder was necessary. The 2θ angle was scanned at a rate of $4^\circ\ min^{-1}$.

XAFS (X-ray absorption fine structure) measurements were performed on the beamline 3Cl (monochromator crystal, Si(111); energy resolution, $\Delta E/E = 2 \times 10^{-4}$; photon flux, 10^9–10^{10} photons $\cdot\ s^{-1}$ in a nonfocused condition) of the Pohang Accelerator Laboratory in Korea. Catalysts calcined at 1123 K were palletized into self-supporting wafers and reduced at various temperatures in a controlled-atmosphere XAFS cell to avoid exposure to air. Ni and Mn K-edge spectra were recorded in a transmission mode at room temperature. Two ionization chambers filled with nitrogen gases were used to measure the incident and the transmitted beam intensities.

The obtained XAFS data were analyzed by using a UWXAFS 3.0 package (27) and FEFF 8.0 code (28), both licensed from the University of Washington. The preedge background was removed by using a simple straight line fitting. The interference function of EXAFS is defined as $\chi(E) = [\mu(E) - \mu_o(E)]/\Delta\mu_o(E_o)$ above the absorption edge (E_o), where $\mu(E)$ is the absorption coefficient due to the particular edge of the element of interest in the sample, $\mu_o(E)$ is the atomlike absorption, and $\Delta\mu(E_o)$ is the jump at the edge. Postedge background function $\mu_o(E)$ is

approximated by a piecewise spline that can be adjusted so that low R components of Fourier transformed data ($\chi(R)$) are optimized. The scaled EXAFS function $k^3\chi(k)$ of the momentum (k) space was converted to the real space, i.e., R space, by Fourier transformation, resulting in the radial structure function (RSF) of the sample. With Fourier filtering, a shell of interest was inversely Fourier transformed into a momentum space, and then, a nonlinear EXAFS fitting was performed. For Ni K-edge, the standard for fitting was a Ni–Ni single scattering synthesized with the FEFF code using available structural parameters for the Ni metal. An adjustable parameter for the fitting, S_o^2, was fixed at 0.86, which was obtained from the curve fitting of experimental data for Ni foil with the theoretical EXAFS equation. For Mn K-edge, the first shell, representing Mn–O interaction, was fitted with Mn–O single scatterings synthesized with the FEFF code using structural parameters of $MnAl_2O_4$ (29) and MnO (30).

3. RESULTS

Various Ni-based catalysts were tested for the carbon dioxide reforming of methane in order to examine the effects of supports and preparation methods on the catalytic activity and stability. Catalytic activity and stability were tested at 923 K with a feed gas ratio CH_4/CO_2 of 1 without a diluent gas. According to the thermodynamic calculation done by Gadalla and Bower (31), high-temperature operation, above 1143 K, is needed to prevent carbon deposition when the feed gas ratio of CH_4/CO_2 is 1 and the total pressure is 1 atm. Hence, the reaction conditions employed here are rather severe in terms of carbon deposition. Typical physical properties and reaction data for these catalysts are summarized in Table 1. Coprecipitated

TABLE 1

Characterization and Reaction Data of Ni Catalysts after CO_2 Reforming of CH_4 at 923 K[a]

Catalyst	Initial BET area (m^2/g)	Coke[b] (g C/$g_{catalyst}$)	Initial CO_2 conversion (%)	Stability[c]
17 wt% Ni/Al_2O_3	130	0.731	72.0	Plugging
17 wt% Ni/ZrO_2	25	0.607	70.9	Plugging
17 wt% Ni/CeO_2	11	0.708	67.3	Plugging
17 wt% Ni/La_2O_3	6	0.122	61.7	0.78
17 wt% Ni/MnO	3	0.132	58.6	0.78
Ni–$MnO_x/MnAl_2O_4$	61	0.003	52.3	0.98
$Ni_{0.03}Mg_{0.97}O$	69	0.135	71.2	0.92
5 wt% Ni/Al_2O_3	108	0.256	67.4	0.56
5 wt% Ni/10 wt% MnO/γ-Al_2O_3	99	0.085	74.5	0.90
3 wt% Mn/ICI	24	0.003	46.9	0.92

[a] Catalyst, 200 mg; feed gas $CO_2/CH_4 = 1$, 81.7 μmol/s.
[b] After 25 h of reaction.
[c] The ratio between the CO_2 conversion at 25 h and that at 5 min on stream.

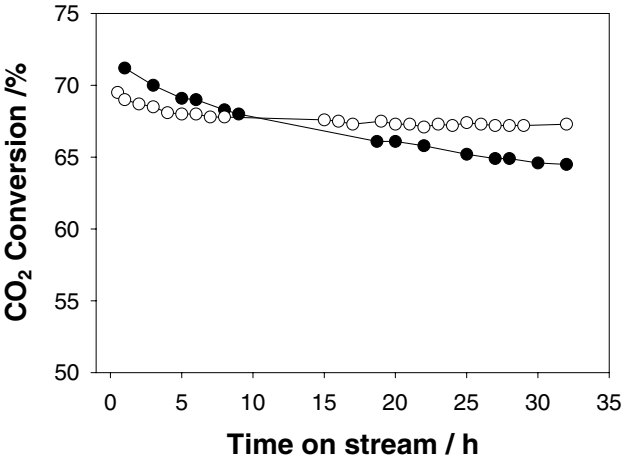

FIG. 1. The comparison of catalytic stability between Ni–$MnO_x/MnAl_2O_4$ —○ and $Ni_{0.03}Mg_{0.97}O$ —● in the carbon dioxide reforming of methane at 923 K and atmospheric pressure. Catalyst, 100 mg; feed gas $CO_2/CH_4 = 1$, 81.7 μmol/s for $Ni_{0.03}Mg_{0.97}O$ and 20.4 μmol/s for Ni–$MnO_x/MnAl_2O_4$.

Ni/Al_2O_3, Ni/ZrO_2, and $NiCeO_2$ showed high initial activities but reactor plugging occurred due to the formation of large amounts of coke. The gradual decrease in the activity was observed for Ni/La_2O_3 and Ni/MnO, in which smaller amounts of coke were formed than in Ni/Al_2O_3, Ni/ZrO_2, and Ni/CeO_2. The catalyst deactivation due to coke formation also occurred for impregnated 5 wt% Ni/γ-Al_2O_3 catalysts. Addition of MnO onto this Ni/γ-Al_2O_3 catalyst decreased the amount of deposited coke drastically and 90% of initial CO_2 conversion was maintained after 25 h of the reaction. $Ni_{0.03}Mg_{0.97}O$, a well-known stable CO_2 reforming catalyst, showed a larger amount of coke deposition but maintenance of activity was as good as 5 wt% Ni/10 wt% MnO/γ-Al_2O_3. The coprecipitated Ni–$MnO_x/MnAl_2O_4$ catalyst showed even more stable catalytic activity and an extremely small amount of coke. The commercial Ni/Al_2O_3 (ICI) modified with 3 wt% Mn also showed a very small amount of coke deposit, yet activity maintenance was not as good as the Ni–$MnO_x/MnAl_2O_4$ catalyst.

To compare the catalyst stability of $Ni_{0.03}Mg_{0.97}O$ and Ni–$MnO_x/MnAl_2O_4$ in a more meaningful way, the carbon dioxide reforming of methane was performed at similar CO_2 conversions by changing the total reactant flow rate. As mentioned, the solid solution of $Ni_{0.03}Mg_{0.97}O$ is one of the most stable nickel-based catalysts known for this reaction (12–17). Coprecipitated Ni–$MnO_x/MnAl_2O_4$ catalyst appeared to be much more stable than $Ni_{0.03}Mg_{0.97}O$ catalyst, as demonstrated in Fig. 1.

Temperature-programmed oxidation (TPO) with 1% O_2/He was performed to probe the properties of deposited carbon. As shown in Fig. 2, the amount of total evolved CO_2 is proportional to the amount of deposited carbon measured by CHNS analyzer. For 17 wt% Ni/Al_2O_3, CO_2

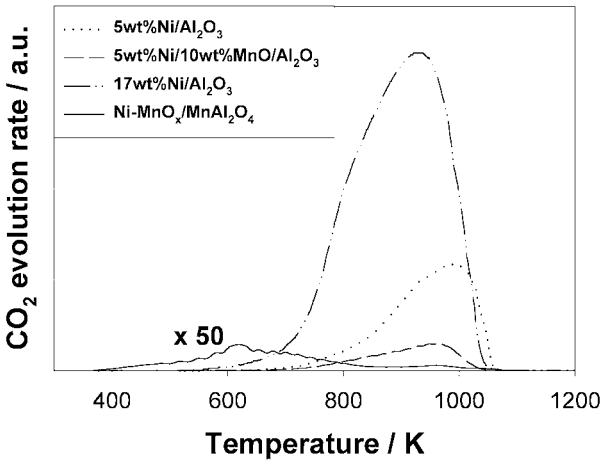

FIG. 2. Temperature-programmed oxidation (TPO) of deposited coke on the catalysts prepared by coprecipitation and impregnation. After 1 h reaction under the same conditions as that for Table 1.

was evolved from 520 to 1070 K. A very small peak around 620 K was observed in the TPO plot for Ni–$MnO_x/MnAl_2O_4$ catalyst. For impregnated 5 wt% Ni/γ-Al_2O_3 and 5 wt% Ni/10 wt% MnO/γ-Al_2O_3 catalysts, CO_2 was produced at higher temperatures, from 670 to 1070 K, and the MnO-modified catalyst showed a much smaller CO_2 peak.

The temperature-programmed desorption (TPD) patterns of CO_2 for Mn-promoted and unpromoted Ni/Al_2O_3 catalysts are compared in Fig. 3. A CO_2-desorption peak at 340 K and a shoulder around 540 K were observed for Ni–$MnO_x/MnAl_2O_4$ catalyst. In contrast, only a single CO_2-desorption peak appeared at 340 K for 17 wt% Ni/Al_2O_3 catalyst. Therefore, the addition of manganese results in the increased amount of adsorbed CO_2.

The electron probe microanalysis (EPMA) was conducted to compare the surface composition of 17 wt% Ni/Al_2O_3 and Ni–$MnO_x/MnAl_2O_4$ catalysts, both of which were prepared by the coprecipitation method. Its quantitative analysis results are presented in Table 2. Both catalysts contain potassium, which is used as a precipitating agent in the catalyst preparation step. In Ni–$MnO_x/MnAl_2O_4$ catalyst, the ratio of Mn/Ni was higher on the catalyst surface, as measured by EPMA, than the bulk composition (1 : 1 atomic ratio).

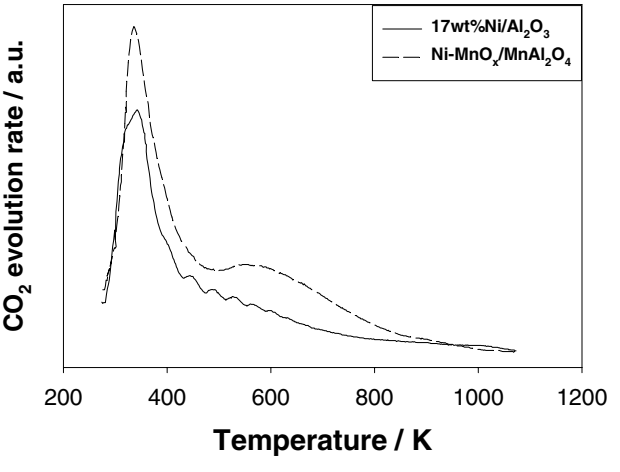

FIG. 3. Temperature-programmed desorption (TPD) of CO_2 on the unpromoted and Mn-promoted catalysts prepared by coprecipitation.

TABLE 2

EPMA Analysis for Coprecipitated 17 wt% Ni/Al_2O_3 and Ni–$MnO_x/MnAl_2O_4$ Catalysts

	17 wt% Ni/Al_2O_3		$NiMnAl_6O_{10}$	
Element	Weight ratio (%)	Atomic ratio (%)	Weight ratio (%)	Atomic ratio (%)
Al	77.0	87.5	56.9	73.0
Ni	21.0	11.0	14.0	8.2
Mn	—	—	23.1	14.5
K	2.0	1.5	6.0	4.3

Coprecipitated Ni–$MnO_x/MnAl_2O_4$ catalyst showed the higher activities with increasing reduction temperatures, as shown in Fig. 4. This trend is in line with metallic nickel surface areas measured with H_2 chemisorption, which were 0.10, 0.54, and 0.78 m^2/g for catalysts reduced at 973, 1073, and 1173 K, respectively. In order to examine change in the bulk structure of this catalyst with reduction temperatures, X-ray diffraction was conducted for coprecipitated Ni–$MnO_x/MnAl_2O_4$ catalysts. Figure 5 shows that dominant bulk crystalline phases are metallic nickel, γ-Al_2O_3, and $MnAl_2O_4$ at all reduction temperatures. As the reduction temperature increased, peak intensities of metallic Ni were strengthened. Intensity of $MnAl_2O_4$ and γ-Al_2O_3 peak was

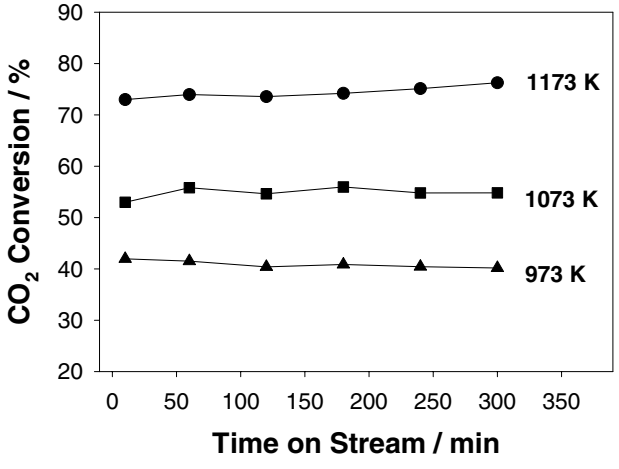

FIG. 4. The effect of reduction temperatures on the catalytic activity in the carbon dioxide reforming of methane at 923 K and atmospheric pressure. Ni–$MnO_x/MnAl_2O_4$ catalyst, 200 mg; feed gas $CO_2/CH_4 = 1$, 81.7 μmol/s.

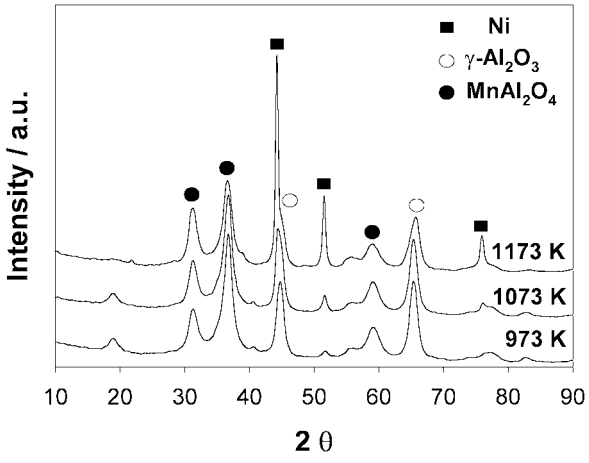

FIG. 5. X-ray diffraction patterns of Ni–MnO_x/$MnAl_2O_4$ catalysts prepared at different reduction temperatures.

not much changed. Ni and Mn K-edge XANES spectra were obtained in order to examine the chemical environment for Ni and Mn of these catalysts prepared at different reduction temperatures. Figure 6 shows Ni K-edge XANES spectra for Ni–MnO_x/$MnAl_2O_4$ catalysts prepared at different reduction temperatures and reference samples of Ni foil and NiO. Easily discernible features of XANES spectra were observed for Ni foil and NiO and the edge energy shift toward a higher energy was an expected result with the increase in the oxidation state of Ni from metallic nickel foil to Ni(II)O. Compared with these reference XANES

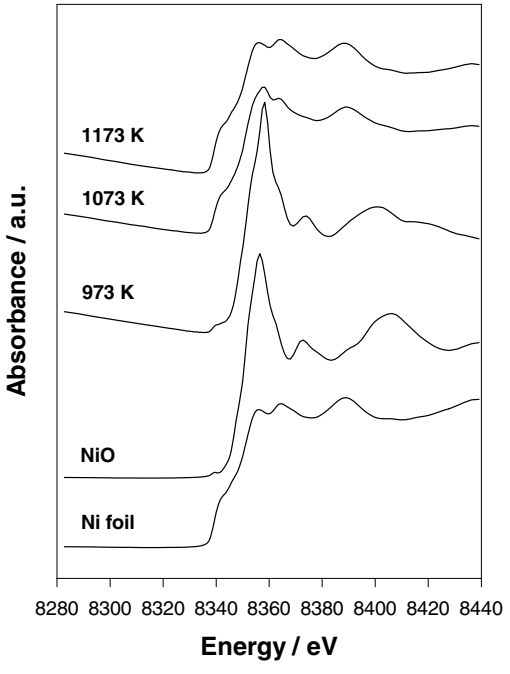

FIG. 6. Ni K-edge XANES spectra for Ni foil, NiO, and Ni–MnO_x/$MnAl_2O_4$ catalysts prepared at different reduction temperatures.

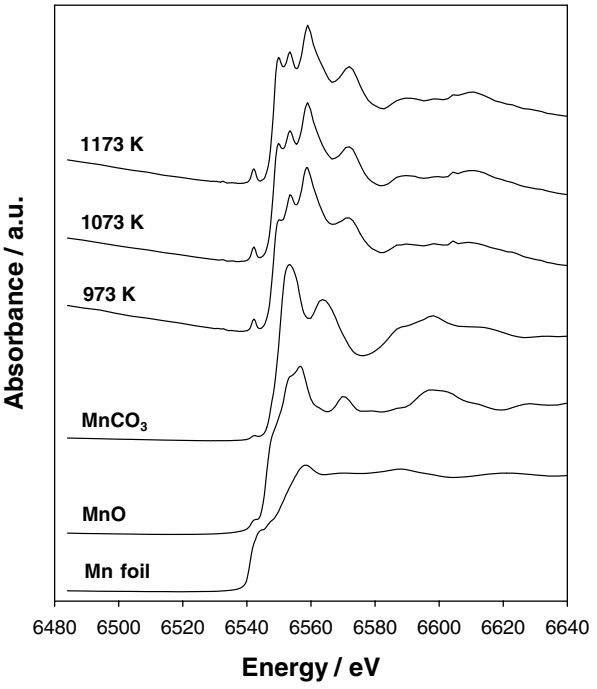

FIG. 7. Mn K-edge XANES spectra for Mn foil, MnO, $MnCO_3$, and Ni–MnO_x/$MnAl_2O_4$ catalysts prepared at different reduction temperatures.

features, it was obvious that nickel was present as NiO in Ni–MnO_x/$MnAl_2O_4$ catalyst reduced at 973 K but that reduced metallic nickel was dominant when it was reduced over 1073 K. Figure 7 shows Mn K-edge XANES spectra of Ni–MnO_x/$MnAl_2O_4$ catalysts prepared at different reduction temperatures and reference samples of Mn foil, MnO, and $MnCO_3$. Ni–MnO_x/$MnAl_2O_4$ catalysts showed that XANES spectra were consistent with none of the reference samples. However, the oxidation state of manganese appeared to be +2, as estimated from the magnitude of edge-energy shift.

Further EXAFS analysis was performed for Ni–MnO_x/$MnAl_2O_4$ catalysts reduced at 1073 and 1173 K to obtain the structural information around Ni and Mn. Ni K-edge EXAFS functions weighted with k^3 and their RSFs for these catalysts are displayed in Fig. 8. For Ni K-edge, both EXAFS function and RSF of Ni–MnO_x/$MnAl_2O_4$ catalysts reduced at 1073 and 1173 K were nearly the same as those for Ni foil, in agreement with the results of XANES described above, and the only difference was the magnitude of spectra. The RSF of Ni K-edge of these catalysts coincided with that of Ni foil up to the fourth shell. Any contribution from manganese as a nearest neighbor did not appear. Experimental EXAFS data was successfully fitted to the theoretical EXAFS equation, as shown in Fig. 9, and the obtained structural parameters were listed in Table 3. In all cases, nickel was present in the metallic state and the coordination number of Ni–Ni increased as the

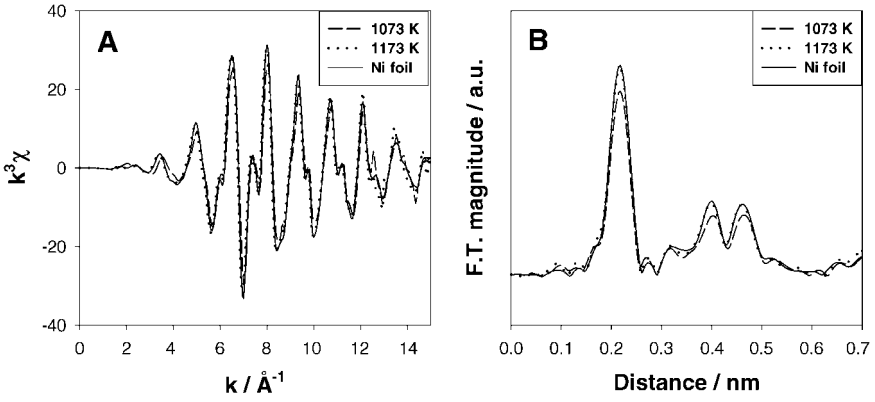

FIG. 8. k^3-weighted EXAFS oscillations of Ni K-edge (A) and its Fourier transforms (B) for Ni–$MnO_x/MnAl_2O_4$ catalysts reduced at 1073 K (dashed line) and 1173 K (dotted line). Those of Ni foil (solid line) were also displayed.

reduction temperature increased. Unlike Ni K-edge, the EXAFS of Mn K-edge was very complicated, as shown in Fig. 10. Peak distances in this plot are not corrected for the phase shift associated with the photoelectron scattering process. Three distinct peaks appeared at distances of 0.10–0.35 nm in RSF. The first peak, around 0.12 nm, is due to Mn–O scattering, which may originate from manganese oxide, and/or Mn–O scattering in $MnAl_2O_4$, whose formation was confirmed with XRD. The peaks around 0.20 nm and 0.30 nm can be assigned as Mn–Mn scattering of MnO and Mn–Al scattering of $MnAl_2O_4$, respectively. EXAFS curve fitting was performed successfully for the first shell (Mn–O), as shown in Fig. 11 and Table 3. As the reduction temperature increased, Mn–O scattering from MnO appeared. This indicates that higher temperatures facilitate the formation of MnO phase.

To improve the Ni/MnO/γ-Al_2O_3 catalyst against coke formation, effects of an additional promoter were investigated, as shown in Table 4. Among basic promoters Mg, Ba, La, Zr, and Ce appeared to improve the catalytic stability and coke resistance without sacrificing the catalytic activity. K-promoted catalyst showed the very stable CO_2 conversions with surprisingly little coke deposited after reaction even though the initial CO_2 conversion was substantially lower than the unpromoted catalyst.

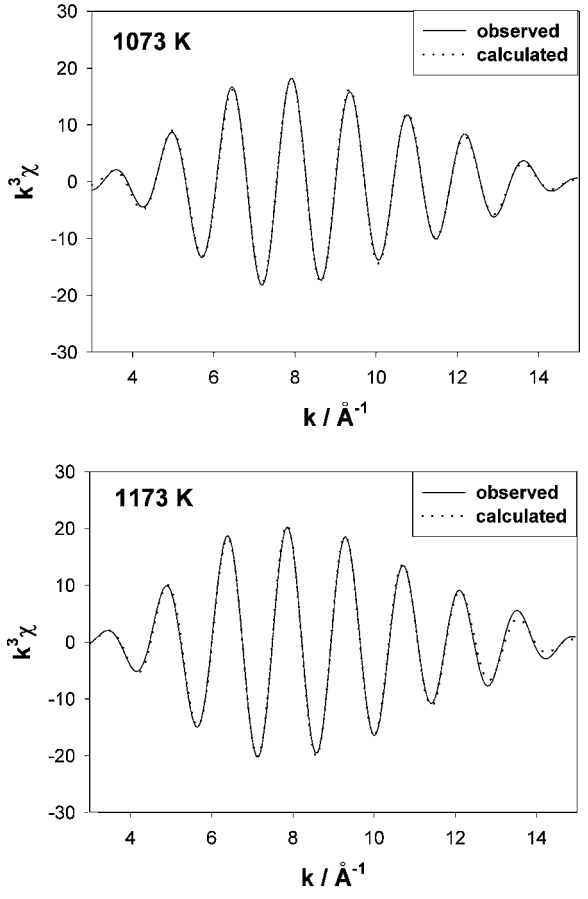

FIG. 9. k^3-weighted Fourier-filtered EXAFS functions of the Ni K-edge for Ni–$MnO_x/MnAl_2O_4$ catalysts reduced at 1073 K (ΔR = 0.114–0.258 nm) and 1173 K (ΔR = 0.114–0.261 nm) fitted to the theoretical EXAFS equation (dotted line). Fitting results were reported in Table 3.

TABLE 3

EXAFS Fitting Results of Ni–$MnO_x/MnAl_2O_4$ Catalysts Reduced at 1073 and 1173 K

Reduction temperature (K)	K-edge	Shell	N	R/Å	σ^2 (Å^2)	R factor[a]
1073	Ni	Ni	9.9	2.488	0.00619	0.00212
	Mn	O	2.48	2.004	0.00508	0.01625
1173	Ni	Ni	11.7	2.496	0.00637	0.00315
	Mn	O	2.63	1.985	0.00441	0.00459
		O	1.63	2.401	0.00336	

[a] R factor gives a sum-of-squares measure of the fractional misfit, which is defined as

$$R = \frac{\sum_{i=1}^{N}\{[\mathrm{Re}(f_i)]^2 + [\mathrm{Im}(f_i)]^2\}}{\sum_{i=1}^{N}\{[\mathrm{Re}(\tilde{\chi}_{data\,i})]^2 + [\mathrm{Im}(\tilde{\chi}_{data\,i})]^2\}}.$$

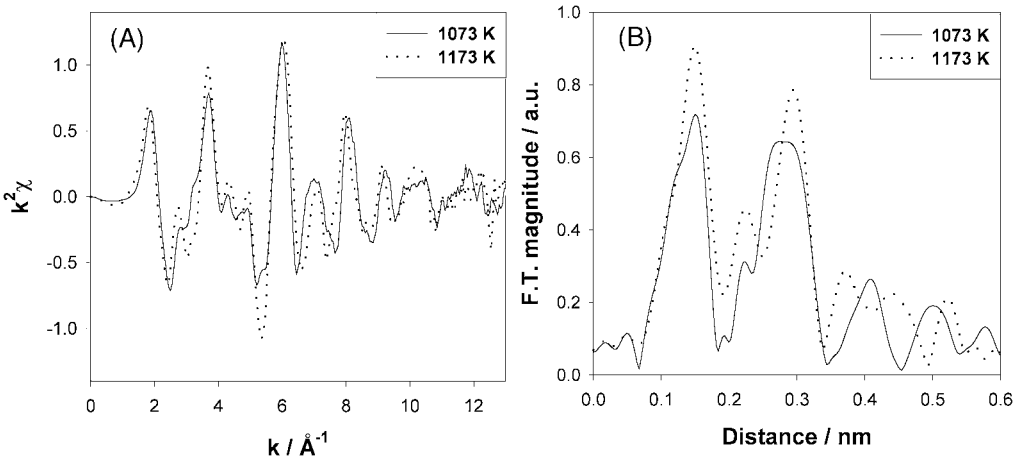

FIG. 10. k^2-weighted EXAFS oscillations of Mn K-edge (A) and its Fourier transforms (B) for Ni–MnO_x/$MnAl_2O_4$ catalysts reduced at 1073 K (solid line) and 1173 K (dotted line).

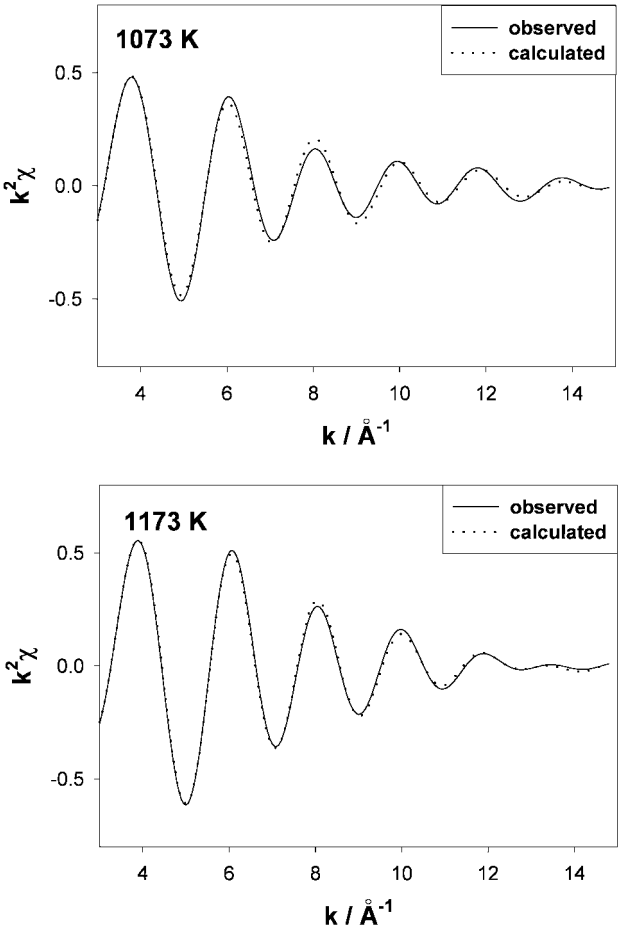

FIG. 11. k^2-weighted Fourier-filtered EXAFS functions of the Mn K-edge for Ni–MnO_x/$MnAl_2O_4$ catalysts reduced at 1073 K (ΔR = 0.068–0.184 nm) and 1173 K (ΔR = 0.068–0.193 nm) fitted to the theoretical EXAFS equation (dotted line). Fitting results were reported in Table 3.

4. DISCUSSION

For dry reforming catalysts, the deactivation could originate from two sources: thermal sintering of nickel and carbon deposition. There was no indication of catalyst sintering under the present reaction conditions, which was supported by the fact that the particle size of metallic nickel calculated from XRD did not change after a reaction. This may be due to the fact that the catalysts were calcined at 973 K and pretreated at 1073 K before the reaction at 923 K. Hence, the deactivation by carbon deposition is believed to be dominant in our case. In our previous works

TABLE 4

Effects of an Additional Promoter (5 wt%) for 5 wt% Ni/10 wt% Mn/Al_2O_3 on the Catalytic Activity and Amounts of Deposited Coke[a]

Additive	Initial CO_2 conversion (%)[b]	Deactivation of CO_2 conversion[c]	Stability[d]	Coke (g C/$g_{catalyst}$)[e]
None	69.9	87.3	92.4	0.081
Na	35.8	92.1	92.1	0.095
K	38.0	99.7	99.7	<0.001
Mg	69.9	91.5	93.6	0.025
Ca	56.1	89.1	91.9	0.030
Ba	63.6	92.8	94.8	0.037
La	68.8	88.3	92.3	0.045
Zr	68.3	93.9	97.4	0.027
Ce	71.2	95.1	96.5	0.026

[a] Reaction conditions: 923 K; 1 atm; catalyst, 100 mg; feed gas CO_2/CH_4 = 1, 81.7 μmol/s.

[b] After 1 h of reaction.

[c] The ratio between the CO_2 conversion at 10 h and that at 1 h on stream.

[d] The ratio between the CO_2 conversion after 3640 mmol of CO_2 converted and that at 1 h on stream.

[e] After 10 h of reaction.

(23, 24), manganese was found to be unique as a promoter for Ni/Al_2O_3 catalysts in suppressing the catalyst deactivation by coke deposition without sacrificing much activity in CO_2 reforming of methane. In these previous works, the impregnation method has been utilized for the preparation of Mn-promoted Ni/Al_2O_3 catalysts but recently we found that the resistance against coke formation could be improved further by adopting the coprecipitation method (25). Here, effects of the preparation method for Mn-containing Ni/Al_2O_3 catalyst on the catalytic activity and stability are discussed.

Mn-promoted Ni/Al_2O_3 catalysts and $Ni_{0.03}Mg_{0.97}O$ catalysts appeared to be most promising among Ni-based catalysts for stable CO_2 reforming of methane. The optimized catalyst prepared by the impregnation method with respect to the chemical composition, impregnation sequence, calcination, and reduction temperatures (25) is 5 wt% Ni/10 wt% MnO/γ-Al_2O_3. This catalyst has the comparable catalytic activity and coke resistance to the well-known $Ni_{0.03}Mg_{0.97}O$ catalyst. However, the gradual decrease in the catalytic activity and small amounts of deposited coke were observed in both catalysts under the present reaction conditions. The $Ni_{0.03}Mg_{0.97}O$ catalyst did not show any loss in activity at 1123 K, $CO_2/CH_4 = 1$, and 1 atm in the original report (14). As mentioned our reaction conditions of 923 K, $CO_2/CH_4 = 1$ at 1 atm is thermodynamically more favorable for coke deposition (12). Compared with these catalysts, coprecipitated $Ni–MnO_x/MnAl_2O_4$ catalysts had much more stable catalytic activity and surprisingly small amounts of deposited coke after reaction under rather severe reaction conditions in terms of coke deposition employed in this study. This stable catalytic activity was also preserved at high CO_2 conversions.

Several techniques, such as TPO, TPD, H_2-chemisorption, XRD, XANES, and EXAFS, have been employed to characterize coprecipitated $Ni\text{-}MnO_x/MnAl_2O_4$ catalysts and to compare them with impregnated $Ni/MnO/\gamma$-Al_2O_3 catalysts. In the temperature-programmed oxidation experiment, the peak of CO_2 evolution over used coprecipitated $Ni–MnO_x/MnAl_2O_4$ catalyst was much smaller and observed at lower temperatures than for impregnated $Ni/MnO/\gamma$-Al_2O_3 catalysts. Thus deposited carbon on $Ni–MnO_x/MnAl_2O_4$ catalyst is not only smaller in amount but also more reactive than that formed on $Ni/MnO/\gamma$-Al_2O_3 catalysts (32). In temperature-programmed desorption of CO_2, a larger amount of CO_2 was desorbed from $Ni–MnO_x/MnAl_2O_4$ catalyst than from 17 wt% Ni/Al_2O_3 catalyst. Both catalysts were prepared by the coprecipitation method. Therefore, addition of manganese results in the increased amount of adsorbed CO_2. The same trend was also observed for impregnated $Ni/MnO/\gamma$-Al_2O_3 catalysts. The moderate basicity of MnO seems responsible for the increased adsorption of CO_2 for promoted catalysts because CO_2 is an acidic gas. It has been reported that the CO_2 desorption peak at higher temperatures represents the presence of the stronger base centers and that the increase in base strength on the surface of catalysts can inhibit carbon deposition (33).

For $Ni–MnO_x/MnAl_2O_4$ catalyst, the catalytic activity increased with an increase in reduction temperatures, which appeared to be closely related to the exposed metallic nickel surface area as observed by H_2 chemisorption. Thus H_2 chemisorption increased with the reduction temperature. Bulk structures observed with XRD were $MnAl_2O_4$ and γ-Al_2O_3 for all reduction temperatures. Regarding nickel phases, the metallic Ni was observed only in $Ni–MnO_x/MnAl_2O_4$ catalysts reduced at high temperatures over 1073 K and its peak intensity increased with increasing reduction temperatures. From XRD line broadening, the particle size of nickel for the sample reduced at 1173 K could be calculated to be 16 nm. Assuming the hemispherical shape, the corresponding metallic nickel surface area is 5.6 m^2/g. This value is far larger than the estimated surface area from H_2 chemisorption (0.78 m^2/g). This confirms that a large part of the surface Ni atoms is blocked by MnO_x, as was proposed for impregnated 5% Ni/10% MnO/Al_2O_3 (24). Such a partial blockage of nickel surface would suppress the coke deposition because the ensemble size necessary for carbon formation is larger than that required for methane reforming (4). Ni K-edge XANES spectra give us information on the oxidation state of nickel in $Ni–MnO_x/MnAl_2O_4$ catalysts reduced at different temperatures. Nickel in $Ni–MnO_x/MnAl_2O_4$ catalyst reduced at 973 K was present mainly as NiO. Above 1073 K, nickel was fully reduced into the metallic nickel. Mn K-edge XANES spectra also show that the oxidation state of manganese was +2. Because Mn K-edge XANES spectra of the catalyst show different patterns compared with divalent manganese reference compounds, FEFF analysis was conducted to generate XANES pattern from crystal data of $MnAl_2O_4$ which was proved to be the dominant manganese phase by XRD. Figure 12 shows the calculated XANES pattern of $MnAl_2O_4$ and MnO. Compared with the observed and calculated XANES spectra, we could conclude that manganese does not form a single phase and that $MnAl_2O_4$ is the dominant phase. Ni K-edge EXAFS analysis shows that the coordination number of Ni–Ni increased with the reduction temperatures and that there is no noticeable direct interaction between Ni–Mn. Mn K-edge EXAFS reveals that interactions of Mn–O, Mn–Mn, and Mn–Al are present. The Mn–O interaction is derived from $MnAl_2O_4$ and/or MnO. Thus, MnO appears to be the species that blocks a part of the nickel surface and, thereby, suppresses the coke deposition. The MnO particles must be very small or, more probably, form patches on large nickel particles, as indicated by the small EXAFS coordination number and total absence of its XRD peaks.

Compared with impregnated $Ni/MnO/\gamma$-Al_2O_3 catalysts, coprecipitated $Ni–MnO_x/MnAl_2O_4$ catalysts showed the very stable catalytic activity and strong coke resistance

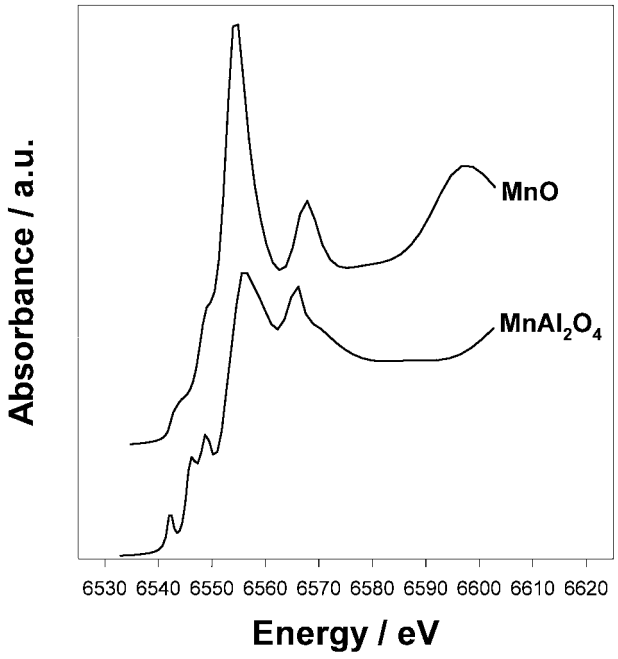

FIG. 12. Theoretically calculated XANES spectra with FEFF 8.00 for MnO and $MnAl_2O_4$.

while having lower initial activities. The big difference in the two catalysts is the amount of potassium retained after preparation. Thus the behavior of the Ni/MnO/γ-Al_2O_3 catalysts doped with additional potassium appeared to be the same in catalytic activity and stability against coke formation as the coprecipitated Ni–MnO_x/$MnAl_2O_{40}$ catalysts. In fact, there was not much difference in the structure and coordination environment of the nickel and manganese contained in the two types of catalysts. One might ask if potassium alone, without manganese, could suppress coke deposition effectively. This does not appear to be the case. The ICI 46-1 catalyst with a composition of NiO (22 wt%), CaO (13 wt%), K_2O (6.5 wt%), SiO_2 (15 wt%), MgO (12 wt%), and Al_2O_3 was not that effective for suppressing coke formation under the present reaction conditions even though it contains a large amount of alkali and alkali earth metal oxides as promoters (23). Therefore, we can conclude that both manganese oxide and potassium should be present as promoters in order to develop a stable nickel catalyst for carbon dioxide reforming of methane.

Some of the additives in Table 4 are well-known to form carbonate (34). For example, K_2CO_3 is stable even at 923 K. The change of Gibbs free energy for the reaction $K_2O(s) + CO_2(g) = K_2CO_3(s)$ is -252.6 KJ/mol. However, from the CHNS analysis, less than 0.001 g C/g catalyst was detected. This is much smaller than the amounts of carbon (0.008 g C/g catalyst) expected if all potassium is present as K_2CO_3. Thus, the formation of bulk carbonate during the reaction appears insignificant. It is known that Na_2CO_3 is less stable than K_2CO_3 (ΔGf (923 K) $= -187.0$ KJ/mol) and $MgCO_3$ is even unstable at 923 K (ΔGf (923 K) $= 40.8$ KJ/mol). Therefore, the contribution of bulk carbonate to CHNS analysis (Table 4) and TPO (Fig. 2) can be negligible.

5. CONCLUSION

The addition of manganese onto an alumina-supported nickel catalyst for the carbon dioxide reforming of methane stabilizes the catalytic activity by suppressing the formation of coke. A coprecipitated catalyst, Ni–MnO_x/$MnAl_2O_4$, showed higher coke resistance and more stable activity than an impregnated Ni/MnO/γ-Al_2O_3 catalyst. However, Ni/MnO/γ-Al_2O_3 catalysts showed a higher initial activity than Ni–MnO_x/$MnAl_2O_4$ catalysts. The coprecipitated Ni–MnO_x/$MnAl_2O_4$ catalyst showed more stable activity and less coke formation rate than the well-known $Ni_{0.03}Mg_{0.97}O$ catalysts at the same CO_2 conversion. XRD revealed that $MnAl_2O_4$, γ-Al_2O_3, and Ni(0) were major crystalline phases and EPMA showed that potassium was present on the surface. Results of XRD, H_2 chemisorption, and XAFS indicated that the surface of large metallic nickel particles was partly covered with patches of MnO and that this structure of manganese oxide accounts for its role in suppressing coke deposition. For impregnated Ni/MnO/γ-Al_2O_3 catalysts, addition of potassium stabilizes further its catalytic activity by suppressing the formation of coke. These results indicate that very stable Ni/Al_2O_3 catalysts for the carbon dioxide reforming of methane can be prepared by addition of both potassium and manganese as promoters.

REFERENCES

1. Houghton, R. A., and Woodwell, G. M., *Sci. Am.* **260**, 36 (1989).
2. Vannice, M. A., *Catal. Rev.–Sci. Eng.* **14**, 153 (1976).
3. Edwards, J. H., Do, K. T., Maitra, A. H., Schuck, S., and Stein, W., *Sol. Eng.* **1**, 389 (1995).
4. Bradford, M. C. J., and Vannice, M. A., *Catal. Rev.–Sci. Eng.* **41**(1), 1 (1999).
5. Ashcroft, A. T., Cheetham, A. K., Green, M. L. H., and Vernon, P. D. F., *Nature* **352**, 225 (1991).
6. Rostrup-Nielsen, J. R., and Hansen, J.-H. B., *J. Catal.* **144**, 38 (1993).
7. Vannice, M. A., and Bradford, M. C. J., *Appl. Catal. A* **142**, 73 (1996).
8. Zhang, Z., and Verykios, X. E., *Appl. Catal. A* **138**, 109 (1996).
9. Wei, J. M., Xu, B. Q., Li, J. L., Cheng, Z. X., and Zhu, Q. M., *Appl. Catal. A* **196**(2), L167 (2000).
10. Horiuchi, T., Sakuma, K., Fukui, T., Kubo, Y., Osaki, T., and Mori, T., *Appl. Catal. A* **144**, 111 (1996).
11. Chen, Y. G., and Ren, J., *Catal. Lett.* **29**, 39 (1994).
12. Gadalla, A. M., and Sommer, M. E., *J. Am. Ceram. Soc.* **72**, 683 (1989).
13. Yamazaki, O., Nozaki, T., Omata, K., and Fujimoto, K., *Chem. Lett.* 1953 (1992).
14. Chen, T.-G., Yamazaki, O., Tomishige, K., and Fujimoto, K., *Catal. Lett.* **39**, 91 (1996).
15. Hu, Y. H., and Ruckenstein, E., *Catal. Lett.* **43**, 71 (1997).
16. Chen, Y.-G., Tomishige, K., Yokoyama, K., and Fujimoto, K., *J. Catal.* **184**, 479 (1999).
17. Tomishige, K., Chen, Y.-G., and Fujimoto, K., *J. Catal.* **181**, 91 (1999).

18. Kim, J.-H., Suh, D. J., Park, T.-J., and Kim, K.-L., *Appl. Catal. A* **197**, 191 (2000).
19. Tang, S., Ji, L., Lin, J., Zeng, H. C., Tan, K. L., and Li, K., *J. Catal.* **194**, 424 (2000).
20. Tomishige, K., Himeno, Y., Matsuo, Y., and Fujimoto, K., *Ind. Eng. Chem. Res.* **39**, 1891 (2000).
21. Nichio, N. N., Casella, M. L., Santori, G. F., Ponzi, E. N., and Ferretti, O. A., *Catal. Today* **62**, 231 (2000).
22. Dibbern, H. C., Plesen, P., Rostrup-Nielsen, J. R., Tottrup, P. B., and Udengaard, N. R., *Hydrocarbon Process.* **65**, 71 (1986).
23. Choi, J. S., Moon, K. I., Kim, Y. G., Lee, J. S., Kim, C. H., and Trimm, D. L., *Catal. Lett.* **52**, 43 (1998).
24. Seok, S.-H., Han, S. H., and Lee, J. S., *Appl. Catal. A* **215**, 31 (2001).
25. Seok, S.-H., MS thesis. Pohang University of Science and Technology, 2000.
26. Moon, K. I., Kim, C. H., Choi, J. S., Lee, S. H., Kim, Y. G., and Lee, J. S., *Hwahak–Konghak*, **35**, 883 (1997).
27. Stern, E. A., Newville, M., Ravel, B., Yacoby, Y., and Haskel, D., *Physica B* **208/209**, 117 (1995).
28. Ankudinov, A. L., Ravel, B., Rehr, J. J., and Conradson, S. D., *Phys. Rev. B* **58**(12), 7565 (1998).
29. Dekker, E., and Rieck, Z., *Z. Anorg. Allg. Chem.* **415**, 69 (1975).
30. Hanawalt, J., Rinn, H., and Frevel, L., *Anal. Chem.* **10**, 457 (1938).
31. Gadalla, A. M., and Bower, B., *Chem. Eng. Sci.* **43**, 3049 (1988).
32. Zhang, Z. L., and Verykios, X. E., *Catal. Today* **21**, 589 (1994).
33. Tang, S. B., Qiu, F.-L., and Lu, S.-J., *Catal. Today* **24**, 253 (1995).
34. Chase, M. W., Jr., Davis, C. A., Downey, J. R., Jr., Frurip, D. J., McDonald, R. A., and Syverud, A. N., "JANAF Thermochemical Tables," 3rd ed., Supp. No. 1, Part I and II, J. Phys. Chem. Ref. Data, Vol. 14. Springer-Verlag, New York, 1985.